

# Experimental investigations and numerical simulations of the mechanical behaviour of polyamides

## Extended abstract

PhD Student: **Eng. Dan-Andrei ȘERBAN**  
Coordinator: **Prof. Dr. Eng. Liviu MARȘAVINA**

This work analyzes the behaviour of a polyamide based semi-crystalline thermoplastic polymer subjected to different types of loadings (tensile, bending, puncture) and different test regimes (static, cyclic, dynamic, low-cycle fatigue). The gathered experimental data was used to design three material models for finite element analysis: hyperelastic formulation, elasto-plastic formulation and viscoelastic formulation. The thesis is divided into six chapters and annexes.

**Chapter 1** represents the thesis' **Introduction** and is divided into three paragraphs. The first paragraph presents a background of polymeric materials briefly describing their structures, properties and exploitation throughout history. The second paragraph deals with the state of the art in polymer characterisation and modelling presenting the main mathematical models used in simulating polymer behaviour to various types of loadings. The third paragraph presents the objectives of the thesis.

**Chapter 2** entitled **Experimental procedures** is divided into five paragraphs and details the experimental procedures that were performed in order to determine the mechanical characteristics of the studied polyamide.

The first paragraph presents an overview of the proposed experimental programme. The second paragraph describes the experimental procedures performed in tension. Several test parameters were investigated for different types of loadings, all being performed on ISO 527 dogbone specimens. For monotone tests in tension, the studied parameters were temperature and strain rate. Temperature influence tests were performed in a temperature interval ranging from  $-25\text{ }^{\circ}\text{C}$  to  $50\text{ }^{\circ}\text{C}$  and recorded a 400% increase in Young's modulus and 185% increase in tensile strength (Figure 1). Strain rate influence tests were performed with crosshead travel speeds from 2 mm/min up to 2,000 mm/min (with average strain rates varying from  $0.00028\text{ s}^{-1}$  to  $0.28\text{ s}^{-1}$ ) and recorded a 30% increase in Young's modulus and a 20% increase in tensile strength (Figure 2).

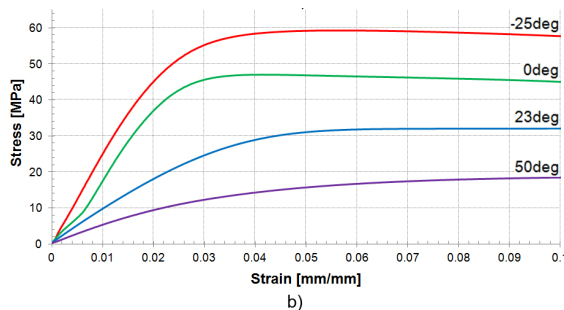


Figure 1. Stress-strain curves for temperature dependency tests performed at 200 mm/min

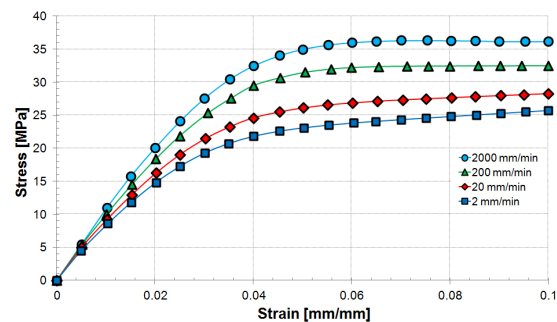


Figure 2. Stress-strain curves strain rate dependency tests performed at room temperature

Cyclic tests were performed with three programmes: the first experimental programme consisted of three blocks of different amplitudes with 10 cycles being performed in each block; the second experimental programme consisted of 10 cycles set in load control having equal stress increment; the third experimental programme consisted of 10 cycles set in strain control

having equal strain increment. From these tests, Mullins effect characteristics were identified: strain softening (material becomes softer when loaded for several cycles at the same amplitude), strain hardening (after being previously subjected to cyclic deformation, further straining will determine the material to resume the stress-strain curve determined by a virgin specimen) and hysteresis (de different paths determined by the loading and unloading curves of cyclic deformations due to energy dissipation).

In order to gain insight on the softening behaviour induced by cyclic loadings, low-cycle fatigue tests were performed. Several tests parameters were investigated: the influence of the number of cycles, the influence of frequency and the influence of the level of straining. For all experimental procedures, the material showed similar behaviour: an emphatic softening was recorded after 1000 cycles (around 30%) followed by an unstressed softening for the rest of the cycles (up to 16% from 1000<sup>th</sup> cycle to the 50,000<sup>th</sup>). The other two parameters showed little influence on test results (Figure 3).

Beside LCF tests, creep tests represent another method of investigating long-term effects of loading. For these tests, three levels of pre-loading were chosen (30%, 60% and 90% of yield stress recorded for the 20 mm/min tests) and a test time of 24h. As with cyclic loading tests, significant softening was recorded in the first hour of the test, the compliance curve beginning to plateau towards the end of the tests (Figure 4).

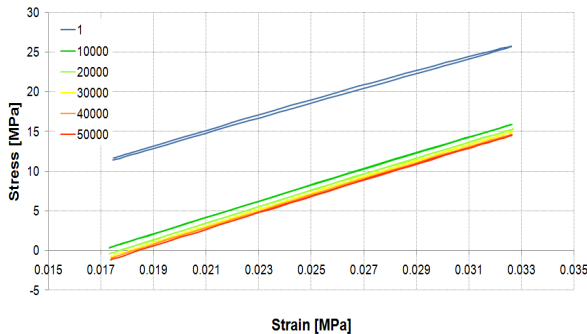


Figure 3. Material softening after 50,000 cycles

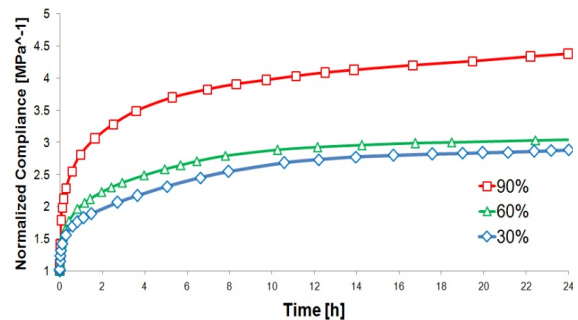


Figure 4. Normalized creep compliance variation with time for three stress levels

Humidity was another parameter whose influence was investigated in tensile loadings. Specimens were conditioned until reaching saturation for 50% relative humidity. Tension tests were performed for three speeds (from 0.00028 s<sup>-1</sup> to 0.28 s<sup>-1</sup>) determining an average softening of 20%.

The third paragraph deals with tests performed in three-point bending. The response of two types of specimens was investigated: the first batch consisted of prism specimens cut from 2mm thick injected plates. Due to the manufacturing process, plates showed residual stresses (investigated with the help o polariscope) (Figure 5) and consequently, dispersion in results was recorded for specimens cut from the same sheet as well as for specimens cut from different sheets (Figure 6).

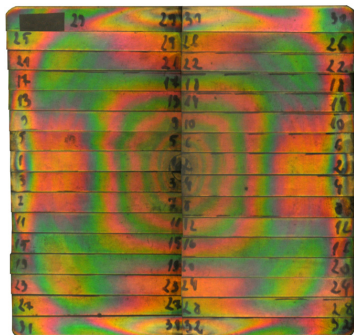


Figure 5. Residual stress distribution for sheets

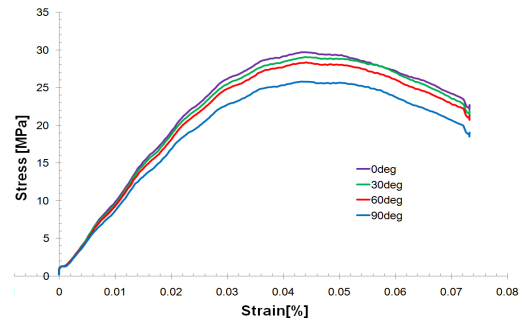


Figure 6. Flow direction influence on flexural properties on sheet specimens

The second batch of specimens consisted of individually injected ISO 527 dogbone specimens tested at crosshead travel speeds ranging from 2 mm/min up to 90,000 mm/min and determined low dispersion of result and more stable response. At high speeds, the influence of stress wave propagation and system ringing had a significant effect on recorded reaction forces (Figure 7).

Due to their ductile behaviour during bending, friction between the specimens and support also influences the reaction forces. Three support types were tested (plastic – metal, plastic – smooth Teflon and plastic – rough Teflon) determining a variation of up to 40% in flexural strength (Figure 8).

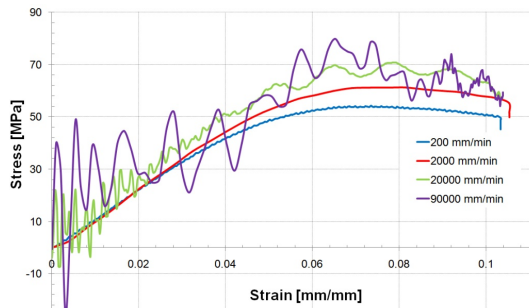


Figure 7. Stress-strain results for dogbone bending tests at various test speeds

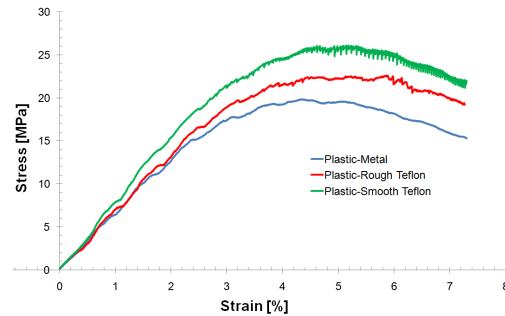


Figure 8. Friction coefficient influence on flexural properties

The fourth paragraph presents the results for the dynamic tests performed on this material, starting with dynamic tests in tension. The tests were performed on a specialised servo-hydraulic machine equipped with a high-speed camera extensometer (Figure 9), at three deformation speeds: 333 mm/s, 667 mm/s and 1000 mm/s (corresponding strain rates of  $2.8 \text{ s}^{-1}$ ,  $5.6 \text{ s}^{-1}$  and  $9.4 \text{ s}^{-1}$ ), the last value being the highest deformation speed which would produce acceptable results. It was observed that apart from the propagation of stress waves throughout the specimens the stress-strain behaviour was identical resulting in the material's saturation.

The second set of dynamic experiments represents Dynamic Mechanical Analysis (DAM) tests and can be classified into two categories: tests performed at low strains (around 0.00001 mm/mm) and tests performed at high strains (up to 0.04 mm/mm). DMA tests at low strains were performed on specialized machines in shear and single cantilever for different frequencies and temperatures. As with tensile tests, temperature has a larger influence on dynamic properties determining a sixfold decrease in storage modulus from  $-30 \text{ }^{\circ}\text{C}$  to  $90 \text{ }^{\circ}\text{C}$  while a frequency variation from 0.1 Hz to 100 Hz determine a 15% increase (Figure 10). DMA tests at high strains were performed on a servo-hydraulic machine in tension. The effect of frequency (from 0.1 Hz to 10 Hz) and strain (from 0.015 mm/mm to 0.043 mm/mm) was investigated determining a 20% increase in storage modulus with frequency and a 10% decrease with strain.

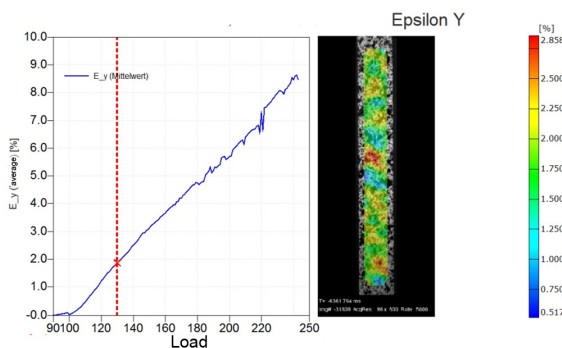


Figure 9. Strain recording with digital image correlation

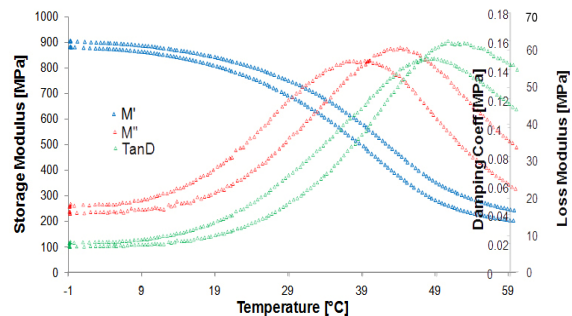


Figure 10. Temperature sweep DMA test at 2 frequencies

The third set of dynamic tests represent puncture impact tests, performed on a specialized impact machine. Two impact speeds were tested (4.4 m/s and 1 m/s) at two temperatures (23 °C and -10 °C). Regardless of the test temperature, the puncture energy was the same (37 J) though the behaviour was different: tests at room temperature determined lower reaction forces and higher fracture deformation than tests at low temperature (Figure 11). At room temperature, specimens displayed ductile failure with steady crack growth (Figure 12). At low speeds, samples did not get punctured.

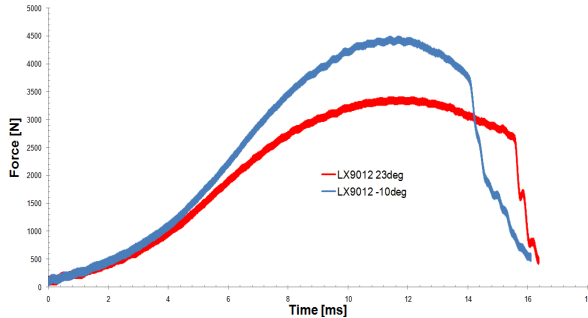


Figure 11. Force-time diagram for puncture tests at two temperatures

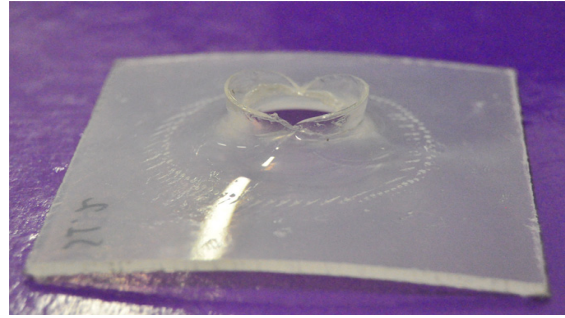


Figure 12. Punctured specimen displaying ductile failure with steady crack growth

The fifth paragraph details the experimental investigations performed on footwear components in modes of deformation similar to what the component encounter in service, namely compression and low cycle fatigue in compression (Figure 13). The influence of strain rate was studied for four crosshead travel speeds (2 mm/min, 20 mm/min, 200 mm/min and 2000 mm/min) determining a 60% variation in compressive properties (Figure 14). Low cycle fatigue tests were performed at 5 Hz for 5,000 cycles determining similar results to LCF tests in tension (a significant softening after 1000 cycles). The influence of humidity was also studied in both compression and LCF. Compression tests determined a 20% softening while LCF tests resulted in similar behaviour.

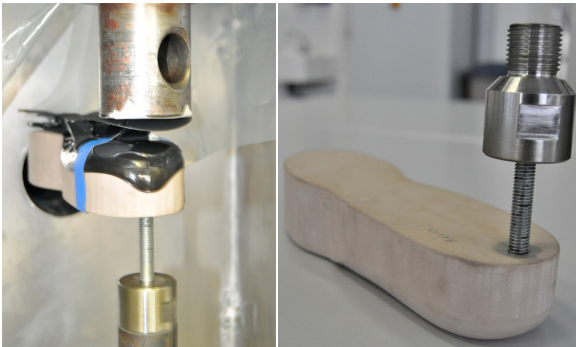


Figure 13. Component testing setup

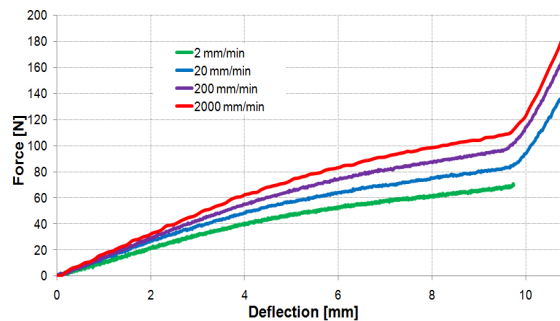


Figure 14. Test speed influence on components' compressive properties

**Chapter 3** entitled **Analytical models for describing material behaviour** is divided into four paragraphs and presents mathematical models used by numerical analysis software as constitutive equations for simulating material behaviour for various types of loading. The first constitutive model presented is linear elasticity through the generalized Hooke law. Considering their components, several types of elasticity tensors are presented: general anisotropic material, monoclinic materials, orthotropic materials, tetragonal materials, cubic materials and isotropic materials.

The second paragraph describes hyperelasticity in terms of a strain-energy density function (a stored elastic potential) and constitutive relations between stress tensors, strain tensors and elasticity tensors for the two descriptions: material description, where the Lagrangian elasticity tensor links the Piola-Kirchhoff stress tensor to the Green-Lagrange strain

tensor and the spatial description for which the Eulerian elasticity tensor links the Trussdell stress rate tensor to the spatial rate of deformation tensor. The way to define hyperelasticity in principal directions was also presented along with formulations for some hyperelastic functions developed over the years: the Mooney-Rivlin model, the neo-Hooke model, the Yeoh model, the Ogden model, the Arruda-Boyce model, the van der Waals model and the Marlow model.

The third paragraph presents some notions of plasticity, introducing the von Mises yield criterion along with two hardening laws: isotropic hardening and kinematic hardening.

The fourth paragraph describes linear viscoelasticity and some formulations based on the two mathematical models (the spring which accounts for linear elasticity and the dashpot that accounts for linear viscosity): the Maxwell fluid (spring and dashpot connected in series), the Kelvin solid (spring and dashpot connected in parallel) and the Voigt-Kelvin solid (Kelvin model and spring connected in series).

**Chapter 4** entitled **Numerical simulations** is divided into four paragraphs, starting with a simulations overview which presents the tests programme and models used in simulations: tensile simulations in monotone and cyclic loadings were performed on a prismatic model with first order tetragonal elements and three-point bending simulations performed on a dogbone model made of second order tetragonal elements.

The second paragraph describes the hyperelastic material model. Several strain-energy density functions were fitted with tensile experimental data, the Marlow potential being the only one that can describe accurate results. Cyclic loading simulations determined accurate results with the help of the Mullins effect sub-option (which is responsible for modelling the unloading behaviour) (Figure 15). Three point bending simulations determined lower reactions regardless of the chosen test speed. In case of dynamic bending, the shape of the force-deflection curve is similar in terms of stress wave propagation but the reactions are lower (Figure 16).

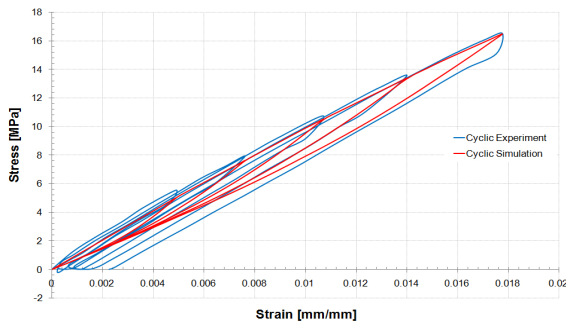


Figure 15. Experimental and simulated cyclic loadings for hyperelastic material

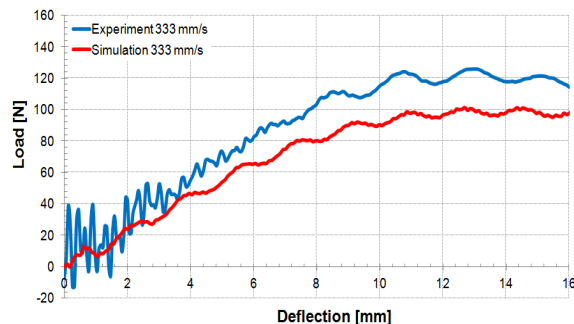


Figure 16. Dynamic three-point bending simulations for 333 mm/s tests

The elasto-plastic formulation is presented in the third paragraph. This model considered Hookean elasticity and rate dependent plasticity for obtaining a strain rate dependent formulation. Both Young's modulus values and yield stress – plastic strain values needed to calibrate the model were determined from tensile stress-strain curves for different rates of deformation and temperature (Figure 17), determining accurate results (Figure 18). Cyclic loading simulations determine inaccurate results due to overestimation of plastic strain (all deformation is considered to be plastic, neglecting viscous effects). As with the hyperelastic model, the elasto-plastic model determines softer reactions regardless of the test parameters in three point bending simulations.

The fourth paragraph presents the viscoelastic material model. Two software implemented forms of viscous function calibration were tested (based on DMA and creep data) all yielding inaccurate results in strain rate dependency tests. In order to obtain an accurate rate-dependent model, a custom relaxation curve was designed based on instantaneous normalized relaxation moduli for different time values for tests (Figure 19). Due to the

overlapping of time values for tests at different rates of deformation, the custom relaxation curve can only predict tensile stress-strain behaviour before 4% deformation after which it overestimates the response (Figure 20). Cyclic loading simulations were able to capture all aspects of Mullins effect (strain softening, strain hardening and hysteresis). As with the previous models, the viscoelastic model determines softer reactions regardless of the test parameters in three point bending simulations.

**Chapter 5** is entitled **Conclusions** and summarizes the main results obtained in the research and points out the most notable contributions.

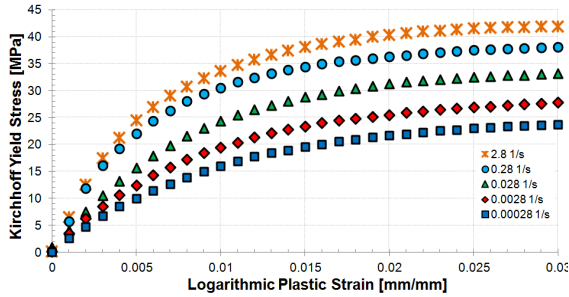


Figure 17. Logarithmic plastic strain variation with Kirchhoff yield stress for five strain-rates at ambient temperature

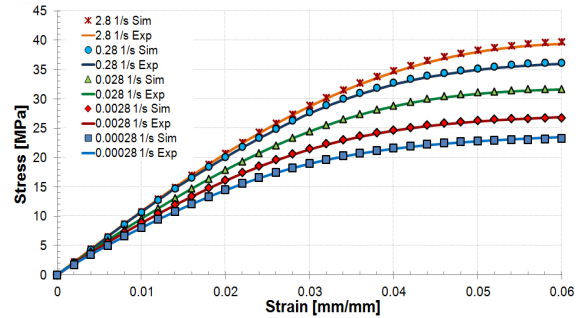


Figure 18. Elasto-plastic material evaluation for static test in tension at 23 °C

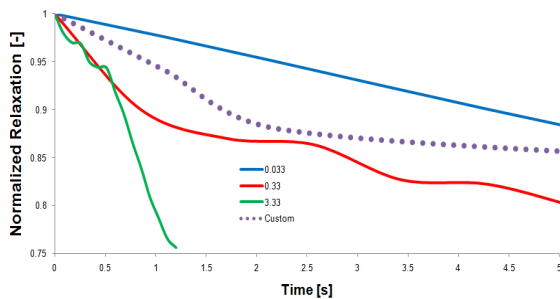


Figure 19. Normalized relaxation functions for different strain rates along with the custom relaxation curve

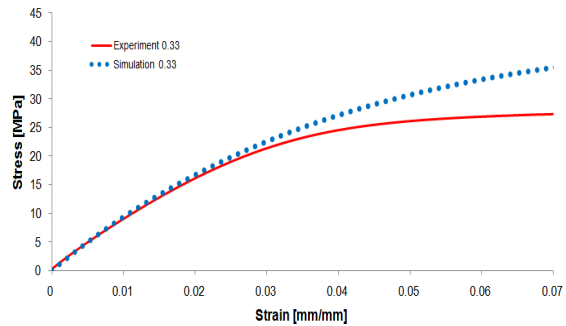


Figure 20. Viscoelastic material simulations for a test speed of 0.33 mm/s